RSC Advances




ROYAL SOCIETY OF CHEMISTRY

www.rsc.org/advances

Cite this: DOI: 10.1039/c0xx00000x

www.rsc.org/xxxxxx

ARTICLE TYPE

# Zinc oxide aerogel-like materials with an intriguing interwoven hollow-sphere morphology for selective ethanol sensing

**Peipei Wang[a], Yongcun Zou[a], Yun Wang[a], Tianrui Chen[a], Jianxiong Gao[a], Ruifei Xuan[b] and Yan Xu*[a]**

***Received (in XXX, XXX) Xth XXXXXXXXX 20XX, Accepted Xth XXXXXXXXX 20XX***
**DOI: 10.1039/b000000x**

**Zinc oxide aerogel-like materials with interconnected multimodal porosity and an intriguing interwoven hollow-sphere morphology were generated from zinc oxide/bacterial cellulose nanocomposite foams by controlled calcination. The monolithic zinc oxide aerogel-like materials with hierarchcial porosity and high specific surface area exhibit excellent selective ethanol sensing properties.**

Inorganic aerogels are a class of porous inorganic polymers in which nanosized blocks are bonded to yield interconnected multimodal porosity, high specific surface area, low density and low thermal conductivity. The monolithic inorganic aerogels allow molecular accessibility, facilitate mass transfer, and optimize specific chemical and physical transformations.[1-3] Since the first report of silica aerogel by Kistler in 1931,[4] a number of inorganic aerogels have been developed exhibiting interesting properties as well as wide-ranging actual and potential applications like cosmic dust collectors, thermal insulators, sensors, catalysts, electrochemical nanodevices, microphotonic devices and for encapsulation of bioactive molecules, *etc*. [2, 5-10]

Zinc oxide is a wide band gap n-type semiconductor holding promises in a variety of applications such as chemical and bio-sensors, optoelectronic devices, catalysis and dye-sensitized solar cells.[11-16] Organizing zinc oxide nanoparticles into a porous architecture affords to enhance functional performance as evidenced by the recent advancement of the field.[14] Aerogels are a special class of porous materials with inherent characteristics beneficial for a variety of applications. It can be anticipated that networking zinc oxide nanoparticles into aerogel architecture likely leads to an advanced set of functional properties. Hope-Weeks et al synthesized zinc oxide aerogel-like materials with an interesting microstructure by using epoxide addition method where metal salts instead of alkoxides were used as precursors. The zinc oxide aerogel-like materials exhibite significant increase in photoluminescence while retaining the inherent characteristics of aerogels like high surface area, low density and open porosity.[17] The synthesis is accomplished in two weeks *via* a multi-step process. Polarz et al prepared zinc oxide aerogel using a carefully controlled sol-gel process from organometallic precursors ($ZnMe_2$, $[MeZnOR]_4$) in a mixed water/diglyme medium followed by solvent extraction using supercritical $CO_2$.[18] The construction of zinc oxide aerogel proceeds from primary particles to secondary aggregates forming a hierarchical porous architecture based on zinc oxide nanoparticles. It exhibits irregular pores in the range of 30-100 nm, BET surface area of 130-150 $m^2g^{-1}$ and potential application in photocatalysis. Ikkala et al prepared ZnO nanotube aerogels based on atomic layer deposition method on cellulose aerogel template. Post-calcination removes cellulose template and transforms amorphous to crystalline phase, leading to self-supporting aerogels based on the hollow nanotubes of zinc oxide.[19] The BET surface area and porosity of zinc oxide nanotube areogel were not released in the paper. By using ultrafast temperature gradient chemical gas-phase synthesis method, Polarz et al prepared zinc oxide aerogel-like materials. These materials are built on hollow spheres of ZnO nanocrystals with multimodal porosity and BET specific surface area of 75 $m^2g^{-1}$. Key steps (from decomposition to crystallization) in constructing the ZnO aerogel-like materials take place in a deliberately designed high-temperature vessel with precise temperature gradient control and a thermophoretic separator for product collection.[20] This work offers an innovative and precise method for producing small quantity of aerogel-like zinc oxice materials. Compared with other methods of aerogel preparation such as sol-gel synthesis and template synthesis, biotemplate approach offers a facile and versatile strategy for producing inorganic aerogel-like materials with hierarchical architectures and interconnected multimodal porosity. It is a two-step process: (1) organization of inorganic/biomolecular nanocomposites through the self-assembly and mineralization of biomolecular templates and (2) controlled calcination of the nanocomposites to remove biotemplates and generate inorganic aerogel-like materials. The morphology and mesostructures of the nanocomposites can be modulated by tuning the reaction parameters, which renders the tunability of the mesostructural features and properties of inorganic aerogel-like materials. Here, we describe the fabrication of zinc oxide aerogel-like materials by controlled calcination of zinc oxide/bacterial cellulose nanocomposites. The zinc oxide aerogel-like materials are built on the hollow spheres of wurtzite zinc oxide nanocrystals and exhibit the BET surface areas of 80 $m^2g^{-1}$.

We show that the zinc oxide aerogel-like materials exhibit excellent ethanol sensing properties as characterized by ultrafast response and recovery, high ethanol selectivity and good sensing stability.

The zinc oxide (ZnO) aerogel-like materials were generated from a zinc oxide/bacterial cellulose nanocomposite containing 70 wt% of ZnO by controlled calcination, designated as ZnO/BC. ZnO/BC was prepared according to the reported procedures.[21] As shown in Fig. S1a, 1b†, it has a string-beaded morphology where ZnO spheres, constructed from ZnO nanocrystals, are stringed by BC nanofibers. In search of optimal calcination conditions, ZnO/BC was calcined at 450 °C, 550 °C, 650 °C and 750 °C, respectively, with the products designed as ZnO-n where n = 450, 550, 650 and 750. As shown in Fig. 1a, 1b, ZnO-450 and ZnO-550 are aerogel-like as they are monolithic and open porous. ZnO-650 and ZnO-750 are not at all aerogel-like as they have lost the monolithic features of aerogels. ZnO-650 contains aggregated ZnO spheres with diameters around 300 nm and ZnO-750 contains non-spherical aggreated ZnO crystals (Fig. 1c, 1d).

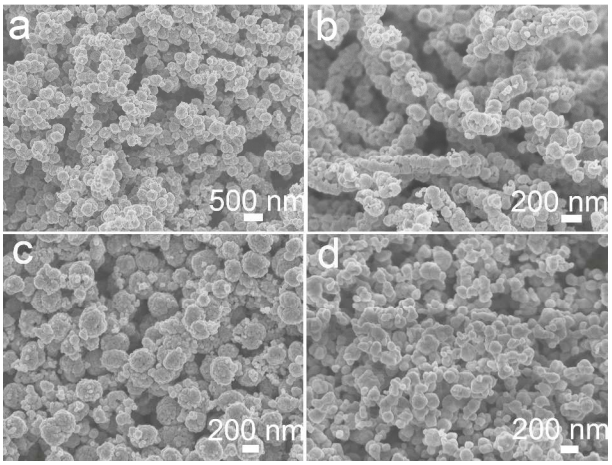


**Fig. 1** SEM images of ZnO-n obtained by calcining ZnO/BC at various temperatures: (a) ZnO-450, (b) ZnO-550, (c) ZnO-650 and (d) ZnO-750.

The morphology of ZnO-450 and ZnO-550 is further characterized using high magnification SEM and TEM. Taking ZnO-550 for example, it is built on ZnO hollow spheres with diameters around 200 nm where the adjacent hollow spheres are interwoven, resulting in an intriguing hollow-sphere morphology (Fig. 2a, 2b). A high magnification TEM image shows that the hollow spheres of ZnO are made of aggregated ZnO nanocrystals with dimensions around 20 nm, on which inter-nanocrystal voids are found (Fig. 2b). The average *d*-spacings of the lattice fringes measured from the HRTEM image are about 0.28 nm and 0.24 nm, agreeing well with those of $d_{100}$ and $d_{101}$ of wurtzite ZnO, respectively (Fig. 2c). Calcination takes place in air, and it causes cellulose to be completely oxidized forming $CO_2$, giving rise to highly crystallized wurtzite ZnO (JPCDS 36-1451, Fig. 2d). The calcination serves dual functions in the formation of the ZnO aerogel-like materials: (1) Removal of the embedded cellulose nanofibers from ZnO/BC and (2) intergrowth of ZnO nanocrystals forming a stable monolithic architecture. The intergrowth among adjacent ZnO nanocrystals is evidenced by TEM and HRTEM imaging analysis (Fig. 2b, 2c). The X-ray diffraction peaks of ZnO are separated and analyzed by a multipeak separation program MDI Jade 5.0.[22] Based on the (100) reflection, the crystallinity of ZnO in ZnO/BC is calculated to be 51% and that in ZnO-550 is about 80% (Fig. 2d). We consider that the intergrowth likely occurs during calcination as a result of crystallization of the amorphous phase in ZnO/BC welding adjacent ZnO nanocrystals together.

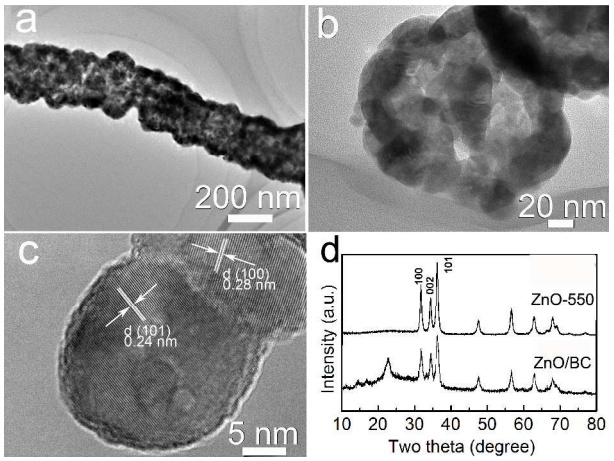


**Fig. 2** (a) High magnification TEM image showing the hollow-sphere morphology of ZnO-550, (b) A high magnification TEM image of ZnO showing that the hollow spheres are made of ZnO nanocrystals with dimensions around 20 nm, (c) HRTEM of ZnO-550 showing the intergrowth between highly crystallized ZnO nanocrystals and (d) XRD of ZnO/BC and ZnO-550 showing that ZnO in ZnO/BC has lower crystallinity than that in ZnO-550.

Slow heating rate and moderate heating temperatures in air are two essential factors determining the construction of stable monolithic and open porous architecture of the ZnO aerogel-like materials based on ZnO hollow spheres. Rapid heating of ZnO/BC at 8 °C $min^{-1}$ instead of 2 °C $min^{-1}$ to 450 °C and 550 °C, respectively, destroys the monolithic architecture, as a result, discrete aggregated nanocrystals of ZnO are produced (Fig. S2†). High temperatures lead to a gradual disappearance of the hollow spheres in favor of the aerogel-like architecture, instead, aggregation of ZnO nanocrystals takes place as in the case of ZnO-650 and ZnO-750 (Fig. 1c, 1d). The ZnO aerogel-like materials contain pure wurtzite ZnO phase and no crystalline impurity is present (Fig. S3†). The crystallinity and the size of ZnO nanocrystals increase with increasing calcination tempreatures as indicated by the intensity and width of the diffraction peaks (Fig. S3†). The sizes of ZnO nanocrystals are about 16 nm and 20 nm for ZnO-450 and ZnO-550, respectively based on the Scherrer equation. Hydroxyl groups are present in ZnO-n whose quantity decreases with increasing calcination temperatures as indicated by the IR absorption peak centered at 3447 $cm^{-1}$ (Fig. S4†).

The nitrogen adsorption-desorption isotherms and BJH pore size distributions of ZnO-n and ZnO/BC are shown in Fig. S5† and Inset. ZnO-450 and ZnO-550 contain meso-macropores with different pore size distributions and the BET surface areas of 65 and 80 $m^2g^{-1}$, respectively. ZnO/BC exhibits the BET surface area of 92 $m^2g^{-1}$ and meso-

macropores. ZnO-550 shows multimodal porosity centered at 30 nm while ZnO-450 and ZnO/BC show broad-featured porosity. A closer inspection of ZnO-550 reveals the presence of inter-nanocrystal voids due to the packing of ZnO nanocrystals. The inter-nanocrystal voids are likely the key contributor of the mesopores while the structural pores circumferenced by welded hollow-sphere and the internal voids of ZnO hollow spheres likely contribute to the formation of macropores in ZnO-550.

The open porous architectures of the ZnO aerogel-like materials with high specfic surface areas and surface-bound oxygen species make the hollow-sphere mesostructures interesting for applications like sensing,[20] catalysis[18] and battery technology.[3] XPS analysis was used to characterize the chemical environment of $O^{2-}$ ions in the ZnO aerogel-like materials. The XPS peak of O1s is asymmetrical and it can be deconvoluated into three component peaks centered around 530.6 eV ($O_L$), 531.8 eV ($O_D$) and 532.6 eV ($O_S$) by fitting to Gaussian function with the area percentage calcuated (Fig. S6†, Table 1). Studies have shown that the $O_L$ and $O_D$ components are associated with the $O^{2-}$ ions in the lattice and in oxygen-deficient regions within the lattice structure of wurtzite ZnO, respectively. The $O_S$ component is attributed to the oxygen species attached to the surface of wurtzite ZnO (chemisorbed, dissociated or $OH^-$).[23, 24] Given that the gas sensing properties of ZnO is closely associated with the $O_S$ component, high percentage of $O_S$ of ZnO-550 might lead to enhanced sensing performance. The ZnO aerogel-like materials were evaluated for gas sensing properties at the optimal operating temperature of 300 °C with the performance comapred with those of reference samples (ZnO-650, ZnO-750 and a commercial ZnO powder, designated as ZnO-coml).

**Table 1**. The deconvoluted XPS O1s peaks of the ZnO materials.

| | Binding Energ (eV) | | | |
|---|---|---|---|---|
| Sampe | $O_L$ | $O_D$ | $O_S$ | $O_S$/O1s* |
| ZnO-450 | 530.6 | 531.8 | 532.7 | 15% |
| ZnO-550 | 530.6 | 531.7 | 532.6 | 19% |
| ZnO-650 | 530.6 | 531.9 | 532.9 | 12% |
| ZnO-750 | 530.6 | 531.8 | 532.7 | 10% |
| ZnO-coml | 530.6 | 531.9 | 532.7 | 10% |

*: $O_S$/O1s: the area percentage of $O_S$ over the total of $O_L$, $O_D$ and $O_S$ deconvoluted from O1s.

The dynamic response-recovery curve of the ZnO-550 sensor shows that the sensor responses and recovers rapidly upon exposure and removal of ethanol as indicated by the sharp signal pickup/drop and the flat baseline in the range of 5-1000 ppm at 300 °C (Fig. 3a). The ZnO-550 sensor exhibits ultrafast response (2 s) and recovery (3 s) for 100 ppm of ethanol (Fig. S7†). The sensitivity of the ZnO-550 sensor to ethanol increases with increasing ethanol concentration as shown by a response of 5, 18, 45 to 5, 50 and 500 ppm of ethanol, respectively (Fig. 3a). The response of the ZnO-550 sensor to 100, 500, and 1000 ppm of ethanol was tested in a 10-day cycle during which the sensor was stored in a sealed desiccator in ambient atmosphere. Little variation has been observed, indicating good sensing stability of the sensor (Fig. 3b). To examine the water adsorption properties of the ZnO-n sensors, TGA was carried out in air in the temperature range of 25 to 800 °C. The weight lose of the ZnO-n sensors between 25 and 300 °C is about 1.0%, suggesting the total amount of absorbed water is low (Fig. S8†). The ethanol sensing performance of the ZnO-550 sensor is greater than those of the reference samples (Fig. 3c). The cross-response of the ZnO-550 sensor was examined by exposing the sensor to 200 ppm of potential interfering gases such as methanol, methylbenzene, acetaldehyde, formaldehyde, ethane, ethylene and benzene at 300 °C. The ZnO sensor exhibits considerably greater response to ethanol than to other gases, showing its excellent selectivity to ethanol gas. The ethanol selectivity of the ZnO-550 sensor is superior to that of the ZnO-coml sensor (Fig. 3d). The ethanol sensing performance of selected ZnO sensors and that of the ZnO-550 sensor is summarized in Table S1.

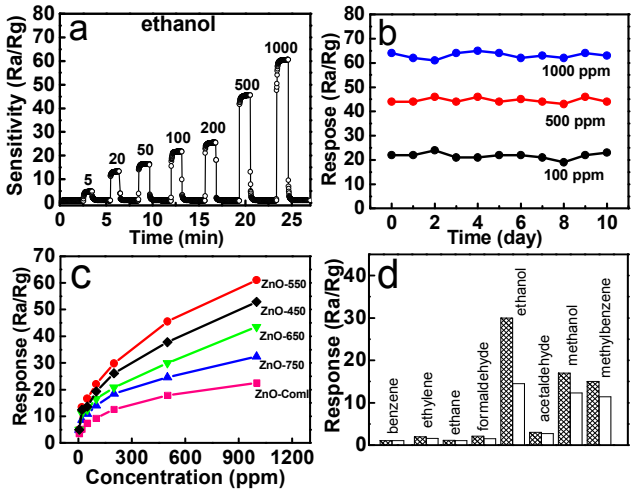


**Fig. 3** (a) Dynamic response-recovery curve of the ZnO-550 sensor to ethanol in the range of 5-1000 ppm at 300 °C, (b) The 10-day stability test of the ZnO-550 sensor to 100 ppm, 500 ppm and 1000 ppm of ethanol at 300 °C, (c) Concentration-response curves of ZnO-550, ZnO-450 and the reference samples to ethanol in the range of 5-1000 ppm at 300 °C and (d) The cross-response of the ZnO-550 and ZnO-coml sensors to 200 ppm of eight different gases at 300 °C (ZnO-550: criss-crossed rectangle; ZnO-coml: open rectangle).

Studies have shown that ethanol sensing performance is mainly affected by following factors: (1) high ethanol adsorption capacity, (2) high specific surface area, (3) high quantity of surface oxygen species and (4) ease of gas diffusion and electron traveling.[23, 25,26] The BET surface areas of ZnO-450, ZnO-650, ZnO-750 and ZnO-coml are 65, 36, 20 and 14 $m^2g^{-1}$, respectively (Fig. S5†), which are significantly smaller than that of ZnO-550 (80 $m^2g^{-1}$). The greater specific surface area allows ZnO-550 better ethanol adsorption capacity. The XPS data shows that ZnO-550 contains the highest percentage of $O_S$ among all tested samples (Table 1), which enables more reactive sites for rapid sensing of reductive gases like ethanol.[23,] The porous hierarchy of ZnO-550 differs from the rest of tested sampels, in that it contains multimodal porosity in the range of 20-100 nm with dominant presence of mesopores centered at 30 nm (Fig. S5b†). Judging from the high BET surface area, we believe that the meso-macropores in ZnO-550 are interconnected that allows easy gas diffusion. Electron traveling through gas sensors largely occurs on surface region that is detrimental for the sensor's

performance.[20] ZnO-550 built on ZnO hollow spheres with thin walls may be composed of great level of depletion leyer to where the movement of the electrons are confined. As a result, the ZnO-550 sensor exhibits greater sensing properties than the rest of ZnO materials.

Controlled calcination of ZnO/BC containing 70 wt% of ZnO results in highly crystallized zinc oxide aerogel-like materials with high BET surface areas and interconnected multimodal porosity. ZnO-550 generated by calcining ZnO/BC at a heating rate of 2 °C $min^{-1}$ to 550 °C exhibits excellent ethanol sensing properties as characterized by ultrafast response and recovery, high selectivity to ethanol and good sensing stability. The current contribution offers a facile approach that may be applicable to the fabrication of a variety of inorganic aerogel-like materials for enhanced functional performance.

## Acknowledgement

This work was supported by the National Natural Science Foundation of China (21171067), Jilin Provincial Talent Funds (802110000412), Tang Aoqing Chair Professor Funds, Jilin University (450091105161), State Key Laboratory of Inorganic Synthesis and Preparative Chemistry, Jilin University (1G3116651461).

## Notes and references

[a]*State Key Lab of Inorganic Synthesis & Preparative Chemistry, Jilin University, Changchun 130012, P. R. China; Tel: 86-431-85168607; E-mail: yanxu@jlu.edu.cn.*
[b]*College of Materials Science and Engineering, China University of Mining and Technology, Xuzhou 221116, China.*

† Electronic Supplementary Information (ESI) available: [details of the experimental section, general characterization, gas sensing measurement and supporting images]. See DOI: 10.1039/b000000x/

1. V. O. Williams, N. C. Jeong, C. Prasittichai, O. K. Farha, M. J. Pellin and J. T. Hupp, *ACS Nano*, 2012, **6**, 6185-6196.
2. A. C. Pierre and G. M. Pajonk, *Chem. Rev.*, 2002, **102**, 4243-4266.
3. T. W. Hamann, A. B. F. Martinson, J. W. Elam, M. J. Pellin and J. T. Hupp, *Adv. Mater.*, 2008, **20**, 1560-1564.
4. L. T. Canham, A. Cullis, C. Pickering, O. Dosser, T. Cox and T. Lynch, *Nature*, 1994, **368**, 133-135.
5. J. M. Wallace, J. K. Rice, J. J. Pietron, R. M. Stroud, J. W. Long and D. R. Rolison, *Nano Lett.*, 2003, **3**, 1463-1467.
6. L. Tong, J. Lou, R. R. Gattass, S. He, X. Chen, L. Liu and E. Mazur, *Nano Lett.*, 2005, **5**, 259-262.
7. N. Hüsing and U. Schubert, *Angew. Chem. Int. Ed.*, 1998, **37**, 22-45.
8. J. L. Mohanan, I. U. Arachchige and S. L. Brock, *Science*, 2005, **307**, 397-400.
9. S. Bag, P. N. Trikalitis, P. J. Chupas, G. S. Armatas and M. G. Kanatzidis, *Science*, 2007, **317**, 490-493.
10. M. A. Worsley, P. J. Pauzauskie, T. Y. Olson, J. Biener, J. H. Satcher Jr and T. F. Baumann, *J. Am. Chem. Soc.*, 2010, **132**, 14067-14069.
11. X. Wang, C. J. Summers and Z. L. Wang, *Nano Lett.*, 2004, **4**, 423-426.
12. P. H. Yeh, Z. Li and Z. L. Wang, *Adv. Mater.*, 2009, **21**, 4975-4978.
13. Q. Zhang, C. S. Dandeneau, X. Zhou and G. Cao, *Adv. Mater.*, 2009, **21**, 4087-4108.
14. T. Yong-Jin Han, M. A. Worsley, T. F. Baumann and J. J. H. Satcher, *J. Mater. Chem.*, 2011, **21**, 330-333.
15. J. El Ghoul, C. Barthou and L. El Mir, *Physica E*, 2012, **44**, 1910-1915.
16. Y. Hong, C. Tian, B. Jiang, A. Wu, Q. Zhang, G. Tian and H. Fu, *J. Mater. Chem. A*, 2013, **1**, 5700-5708.
17. Y. P. Gao, C. N. Sisk and L. J. Hope-Weeks, *Chem. Mater.*, 2007, **19**, 6007-6011.
18. M. Krumm, C. L. Pueyo and S. Polarz, *Chem. Mater.*, 2010, **22**, 5129-5136.
19. J. T. Korhonen, P. Hiekkataipale, J. Malm, M. Karppinen, O. Ikkala and R. H. Ras, *ACS Nano*, 2011, **5**, 1967-1974.
20. S. Dilger, C. Lizandara-Pueyo, M. Krumm and S. Polarz, *Adv. Mater.*, 2012, **24**, 543-548.
21. P. P. Wang, J. Zhao, R. F. Xuan, Y. Wang, C. Zou, Z. Zhang, Y. Wan and Y. Xu, *Dalton Trans*., 2014, **43**, 6762-6768.
22. C. Yi, L. Tian, F. Tang, L. Wang, H. Zou and W. Xu, *Polym. Composites*, 2010, **31**, 933-938.
23. L. Zhang, J. Zhao, H. Lu, L. Li, J. Zheng, H. Li and Z. Zhu, *Sens. Actuators B Chem.*, 2012, **161**, 209-215.
24. S. Bang, S. Lee, J. Park, S. Park, W. Jeong and H. Jeon, *J. Phys. D Appl. Phys.*, 2009, **42**, 235102-235108.
25. H. Zhang, R. Wu, Z. Chen, G. Liu, Z. Zhang and Z. Jiao, *CrystEngComm*, 2012, **14**, 1775-1782.
26. P. P. Wang, Q. Qi, X. Zou, J. Zhao, R. F. Xuan and G. D. Li, *RSC Adv.*, 2013, **3**, 23980-23983.

# Zinc oxide aerogel-like materials with an intriguing interwoven hollow-sphere morphology for selective ethanol sensing

**Peipei Wang[a], Yongcun Zou[a], Yun Wang[a], Tianrui Chen[a], Jianxiong Gao[a], Ruifei Xuan[b] and Yan Xu*[a]**

Zinc oxide aerogel-like materials with interconnected porosity and large specific surface area have been prepared, showing excellent ethanol sensing properties.